

Influence of light-burned spinel on the slag resistance of alumina-spinel refractory castables

Wen Yan^{a,*}, Junfeng Chen^a, Nan Li^a, Wendong Qiu^b, Junhua Ouyang^b and Xiaojun He^b

^aThe State Key Laboratory of Refractories and Metallurgy, Wuhan University of Science and Technology, Wuhan, China

^bRefractories Technology Department, Shanghai Baosteel Industry Technological Service Co. Ltd., Shanghai, China

Slag resistances of alumina-spinel castables containing different types of spinel were investigated using the static crucible test. The corroded samples were characterized using an X-ray diffractometer, a scanning electron microscope, microscopic measurement method etc. Based on the results, the effects of light-burned spinel and commercial fused spinel on the slag resistance of the castables were discussed and compared. It has been found that light-burned spinels could improve the slag penetration resistance of alumina-spinel castable more efficiently than their fused counterparts, if their chemical composition, particle size, lattice distortion extent and grain size are properly controlled. The light-burned spinel containing 70 wt% Al_2O_3 has greater lattice distortion and smaller particle size, making the penetrated slag more viscous and resulting in smaller pore sizes in the matrix. On the other hand, its smaller grain size only results in a slightly higher dissolution rate. Therefore, compared with the fused spinel containing the same amount of Al_2O_3 , it could greatly enhance the slag penetration resistance of the castable while only slightly negatively affecting the corrosion resistance.

Key words: Alumina-spinel castables, Light-burned spinel, Fused spinel, Slag, Corrosion mechanism

Introduction

Alumina-spinel refractory castables have been extensively used as the ladle working linings because of their excellent properties and easy installation [1-18]. Compared with aggregates, the matrix in a castable is more easily corroded by a slag. To improve the properties of the matrices in alumina-spinel castables, two different methods could be used: one is introducing dead-burned spinel (whose sintering temperature was about 1800 °C [1]) or fused spinel (pre-synthesized spinel) into the castable matrix [1-6], and the other is adding magnesia to the castable matrix to form spinel in situ (in-situ spinel) [7-13]. There are some similarities as well as differences between these two methods.

The similarities are in that spinels can enhance the slag penetration resistance of an alumina-spinel castable. When spinel comes in contact with a molten slag, its dissolution rate into the slag is much lower than that of corundum. In addition, spinel can take up MnO/FeO/ Fe_2O_3 from the slag to form complex spinel, increasing the viscosity and melting temperature of the penetrated slag and thus inhibiting the further slag penetration. An Al_2O_3 -rich spinel in particular can accommodate more MnO/FeO/ Fe_2O_3 from the slag because of its many more lattice defects. According to Korgul et al, such a

spinel in the refractory could take up MnO/FeO/ Fe_2O_3 from the slag, making the slag silica-rich and more viscous, thus limiting the slag penetration [1].

The differences are in that the effects of the crystal integrity and grain size of the two types of spinel on the slag resistance are different. The pre-synthesized spinels have better crystal integrity and chemical stability, and thus a lower dissolution rate. In addition, they have better volume stability, and will not lead to cracking in the castables arising from the volume expansion associated with the formation of spinel at high temperatures. However, their accommodation capability of slag ions is relatively low. On the other hand, in-situ spinels have a larger specific surface area, higher activity and greater lattice distortion, compared to the pre-synthesized spinels, so can accommodate more slag oxides such as FeO and MnO; additionally, the formation of an appropriate amount of in-situ spinel from MgO and Al_2O_3 is accompanied with only a certain volume expansion, which may “squeeze” the pores in the castables and inhibit the slag penetration. However, their grain size is relatively smaller, resulting in more readily dissolution into the slag. In addition, it is technically not allowed to introduce too much MgO into the matrix of the castable to form too much spinel in situ, as this would lead to cracking in the castable. On the other hand, it is also difficult to disperse/distribute homogeneously a small amount of MgO. Consequently the uniform distribution of a small amount of in-situ spinel in the castables would not be easily achieved.

Obviously, these two types of spinel have their

*Corresponding author:
Tel : +86-027-68862511
Fax: +86-027-68862121
E-mail: yanwen@wust.edu.cn

respective advantages and disadvantages. Now, one interesting question is that if it is possible to design and use of a “new” type of spinel which inherits the advantages of the two types of spinel while without suffering from their disadvantages. A light-burned spinel synthesized at a relatively low temperature (1600 °C) is a kind of pre-synthesized spinel, but it is different from a dead-burned, fused or in-situ spinel. Compared to a dead-burned or fused spinel, a light-burned spinel has a higher reactive activity and greater lattice distortion, thus can accommodate more slag ions. On the other hand, compared to an in-situ spinel, a light-burned spinel has bigger grain size and better volume stability, and a lower dissolution rate in slag. So, it could be a good candidate spinel which meets the requirements mentioned in the above question. Unfortunately, until now, the effect of a light-burned spinel on the slag resistance of alumina-spinel castables has not been well investigated and fully understood. These now will be addressed in the present paper.

Experimental

Commercial alumina and magnesite powders were used to prepare three types of light-burned spinel. The three powder mixtures were pressed at a pressure of about 100 MPa to form cylindrical samples with 50 mm in height and 50 mm in diameter. The green compacts after drying at 110 °C were fired at 1600 °C for 180 min in an electric furnace. After furnace-cooling to room temperature, the resultant compacts were crushed and then ground to <88 μm powders. The three light-burned spinels were referred to as LS70, LS78 and LS90, respectively. A commercial fused spinel less than 88 μm (referred to as FS70) was used for comparison. The chemical and phase compositions, grain sizes and lattice distortions of the four types of spinels are listed in Table 1. The particle size distributions of these four types of spinel are shown in Fig. 1, and mono-peak modes are observed in their curves. The median particle sizes of LS70, LS78, LS90 and FS70 were 12.57 μm, 14.89 μm, 20.26 μm and 31.67 μm, respectively.

Four types of castables were prepared using the same white fused corundum aggregates but their matrices were different. The particle-size distribution, aggregate content (70 wt%), matrix content (30 wt%) and water content (4.8 wt%) were similar for all batches of the castables. The matrices consisted of 15 wt% corundum powder, 10 wt% spinel powder, 2 wt% α -Al₂O₃ micropowder, 3 wt% calcium aluminate cement and additional 0.6 wt% microsilica. Four castables were referred to as CLS70, CLS78, CLS90 and CFS70 respectively according to their spinel contents (Table 1). The rectangle parallelepiped specimens of 140 mm (length) × 25 mm (width) × 25 mm (thickness) were casted for the porosity measurement. Cubic blocks having holes of 30 mm in diameter and 40 mm in depth were vibrocasted for the crucible corrosion tests. They were cured for 24 h at room temperature prior to drying at 110 °C for a further 24 h. 30 g slag (Table 1) were placed in the hole in a dried sample and heated at 1600 °C for 3h in an electric chamber furnace before furnace-cooling to room temperature.

After the corrosion tests, crucibles were cross-sectioned perpendicularly to the slag-refractory interface, as shown in Fig. 2. The actual corroded and penetrated areas in each sample were measured by the counting

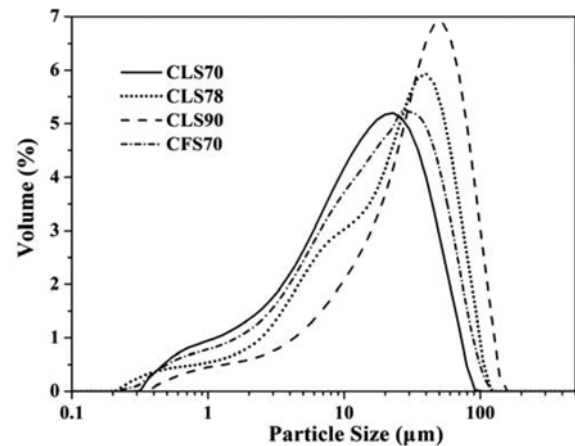


Fig. 1. Particle size distributions of the four spinels.

Table 1. Chemical compositions, mineral phases, properties of the four spinels and chemical composition of the slag.

	Chemical composition (wt.%)									Mineral phases	Grain size (nm)	Lattice distortions (%)
	Al ₂ O ₃	MgO	SiO ₂	CaO	Fe ₂ O ₃	MnO	K ₂ O	Na ₂ O	TiO ₂			
LS70	71.57	26.85	0.55	0.32	0.14	–	0.08	0.08	0.09	Spinel, minor periclase	304	0.131
LS78	78.32	20.34	0.42	0.20	0.33	–	0.08	0.07	0.06	Spinel, minor corundum	122	0.127
LS90	89.28	9.76	0.31	0.15	0.32	–	0.06	0.05	0.03	Spinel, some corundum	121	0.135
FS70	73.40	25.28	0.30	0.46	0.14	–	–	–	–	Spinel	1182	0.098
Slag	0.89	7.91	17.22	47.20	23.77	2.36	0.02	0.04	0.69	–	–	–

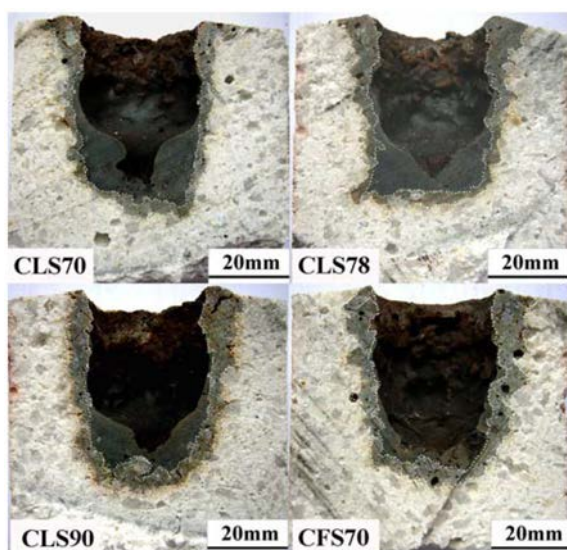


Fig. 2. Photographs of the crucible samples after the slag tests (vertical cut).

pixels method. Corrosion here is defined as the regions of refractory completely replaced by slag. The corrosion index I_C and penetration index I_P are obtained by following equation: $I_{C(P)} = S_{C(P)} / S_O * 100\%$; S_O is the original section area of the crucible inner chamber; S_C is the section area of refractory completely replaced by slag; S_P is the penetrated section area.

Particle size distributions and median particle sizes of the four types of spinel were measured by a laser particle size analyzer (Mattersizer 2000). Apparent porosities of the castables were measured based on the Archimedes' principle using water as the medium. Phase identification was carried out by using an X-ray diffractometer (Philips Xpert TMP) with a scanning speed of 2° per minute. Lattice distortion and grain size of spinel were calculated based on the Scherrer's Law using the X' Pert High Score software. The pore size distribution and median pore size were examined by the microscopic measurement method [19-20] using an optical microscope (Axioskop40). Microstructures of these samples were observed by a scanning electron microscope (Philips, nanoSEM400). The compositions of complex spinels and glass phases in microstructure were determined by calibration with EDAX ZAF quantification (standardless). The viscosities of glass phases at 1600°C were calculated based on the glass phase composition obtained by EDAX, using the Viscosity mode of the FactSage 6.2 thermochemical software.

Results and Discussion

Fig. 3 shows corrosion and penetration indexes of the four castables corroded for 3h at 1600°C . It is found that from castables CLS70 to CLS90, the penetration index increases evidently, whereas the corrosion index

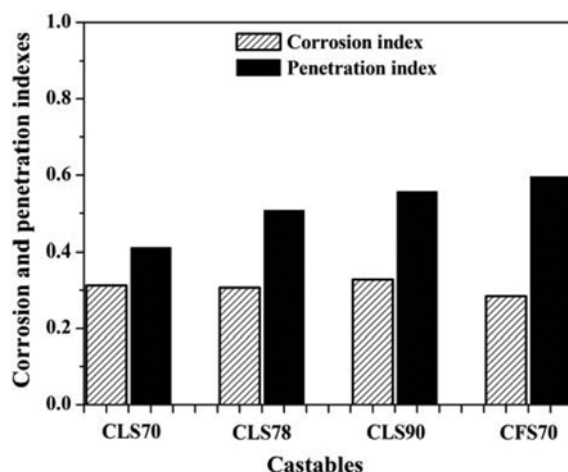


Fig. 3. Corrosion and penetration indexes of the four castables corroded for 3 h at 1600°C .

changes little. Compared with the castables containing light-burned spinels, castable CFS70 containing fused spinel has the highest penetration index and the lowest corrosion index; especially compared with the castable CLS70, the corrosion index of castable CFS70 decreases slightly by 0.028, while the penetration index increases greatly by 0.186.

Obviously, two conclusions could be drawn based on the corrosion testing results shown in Fig. 3 : 1) with increasing the Al_2O_3 content of light-burned spinel the penetration resistance of castable decreases gradually; 2) compared with fused spinel FS70, light-burned spinel LS70 enhances the penetration resistance of castable more efficiently while only slightly negatively affects the corrosion resistance. To understand the strong effects of spinels on the penetration resistances of alumina-spinel castables, two issues need to be considered.

One issue is the possible difference in the slag ion absorbing capacity (SIAC) of these four types of spinel, which would affect the composition and viscosity of the penetrated slag. Microstructures of matrices in the corroded castables CLS70, CLS90 and CFS70 are shown in Fig. 4. The fuscous contrast phases (referred to as S1 to S12) are complex spinels whose EDS results are listed in Table 2. It can be seen that spinels LS70, LS90 and FS70 all have absorbed large amounts of Fe_2O_3 and MnO from the slag. The average contents of ($\text{Fe}_2\text{O}_3 + \text{MnO}$) in LS70, LS90 and FS70 spinels are 21.65 wt%, 20.19 wt% and 14.61 wt%, respectively. There is no obvious difference in the SIAC of the two light-burned spinels, however, the SIAC of light-burned spinel LS70 is remarkably bigger than that of fused spinel FS70 despite their similar chemical compositions. It can be seen from Table 1 that the lattice distortion of spinel LS70 is similar to that of spinel LS90, but greater than that of spinel FS70, this, along with the SIAC values stated above, indicates that the lattice distortion of spinel strongly affects the

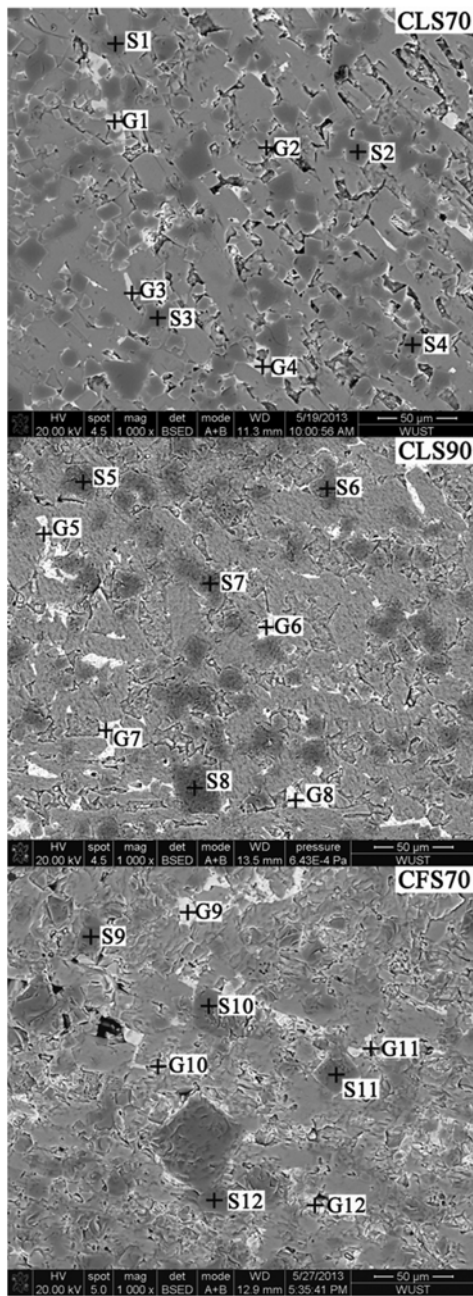


Fig. 4. Typical SEM micrographs of matrices of corroded castables CLS70, CLS90 and CFS70 at the surface of their penetration layers.

spinel's SIAC. The greater the lattice distortion is, the stronger the SIAC of spinel is.

The bright contrast phases (referred to as G1 to G12) in Fig. 4 are glass phases whose EDS results are listed in Table 3. They mainly consist of Al_2O_3 , SiO_2 , CaO and Fe_2O_3 , along with minor MgO and MnO . The SiO_2 and Fe_2O_3 contents of glass phases in castables CLS70 and CLS90 are similar, but different from those in castable CFS90. Spinel LS70 and LS90 in castables absorb more Fe_2O_3 and MnO from the slag, increasing the SiO_2 content of the penetrated slag. Consequently the viscosities of the penetrated slags in castables CLS70 and CLS90 are higher than those in castables CFS70. The higher the viscosity of the slag is, the more difficult the penetration of the slag is. This is the main reason why castable CLS70 shows better slag penetration resistance than castable CFS70.

The other issue that needs to be considered is porosity, as pores are the main channels for the slag penetration. Pore size distributions of matrices of castables CLS70, CLS78 and CFS70 are mono-peak model, whereas pore size distribution of CLS90 is bi-peak model (Fig. 5), indicating that in castables CLS70, CLS78 and CFS70 there are only small pores ($< 30 \mu\text{m}$), whereas in castable CLS90, apart from small pores, there are a few big pores ($40 \sim 200 \mu\text{m}$). Cumulative porous volumes versus pore diameters are plotted in Fig. 6. For the matrices of castables containing light-burned spinels, with increasing the Al_2O_3 content in the spinel the curves shift toward the right-hand side. The curve of castable CFS70 locates between the curves of castables CLS78 and CLS90. Median pore sizes of matrices of four castables and apparent porosities of four castables are shown in Fig. 7. The median pore sizes of matrices of castables CLS70, CLS78, CLS90 and CFS70 are $4.58 \mu\text{m}$, $4.82 \mu\text{m}$, $5.43 \mu\text{m}$ and $5.03 \mu\text{m}$, respectively. And apparent porosities of these four castables are similar, being 11.6%, 11.9%, 11.4% and 11.3%, respectively. Obviously, pore size distribution and median pore size, rather than apparent porosity, reflect the main differences in pore characters of the four castables.

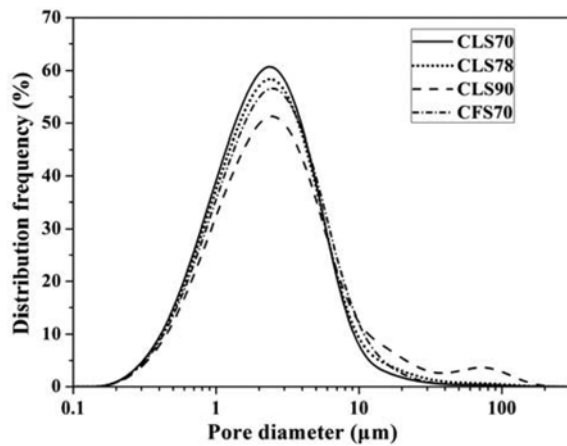
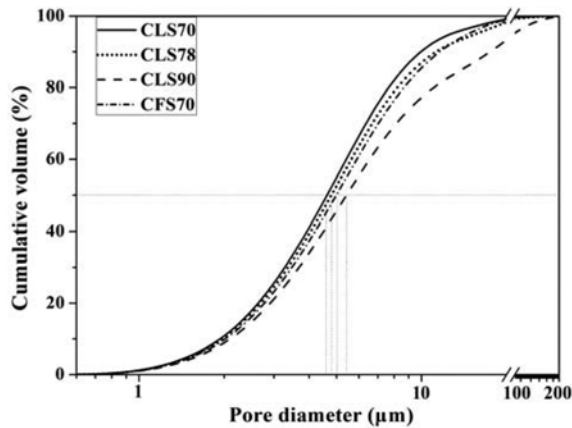
The lattice distortions of spinels LS90 and LS70 used respectively in castables CLS90 and CLS70 are slightly

Table 2. EDS results of composite spinels in Fig. 4 (wt%).

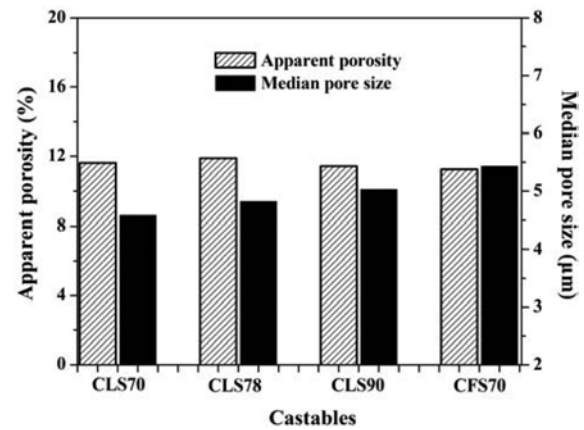
	S1	S2	S3	S4	S5	S6	S7	S8	S9	S10	S11	S12	
EDS results	MgO	22.40	21.79	21.77	22.21	21.42	22.61	20.22	22.55	24.69	24.39	24.19	22.67
	Al_2O_3	55.74	60.66	55.53	53.30	59.70	58.92	56.63	57.19	61.52	62.17	61.65	60.27
	Fe_2O_3	3.43	2.72	2.77	3.42	3.30	3.89	3.15	4.30	1.79	2.12	2.26	2.72
	MnO	18.43	14.83	19.93	21.06	15.58	14.59	20.00	15.96	11.99	11.32	11.90	14.35
	$\text{Fe}_2\text{O}_3 + \text{MnO}$ content	21.86	17.55	22.71	24.49	18.88	18.47	23.15	20.26	13.79	13.44	14.16	17.07
	Average content of ($\text{Fe}_2\text{O}_3 + \text{MnO}$)		21.65				20.19			14.61			

Table 3. EDS results and viscosities at 1600 °C of glass phases in Fig. 4.

	G1	G2	G3	G4	G5	G6	G7	G8	G9	G10	G11	G12
EDS results (wt%)	MgO	0.25	0.00	0.48	0.00	0.00	0.32	0.00	0.00	0.00	0.00	0.00
	Al ₂ O ₃	15.64	17.89	16.32	16.51	16.76	17.02	16.65	16.97	17.44	16.33	16.07
	SiO ₂	27.74	25.64	26.16	26.01	26.93	25.49	25.78	27.10	22.13	22.06	19.53
	CaO	45.24	44.89	45.18	46.69	44.84	45.92	46.24	45.02	46.81	47.05	48.67
	Fe ₂ O ₃	10.89	11.30	11.86	10.38	11.12	11.25	11.05	10.91	13.24	14.56	15.21
	MnO	0.24	0.28	0.00	0.41	0.35	0.00	0.28	0.00	0.38	0.00	0.52
Viscosities (Pa · S)	0.111	0.108	0.106	0.107	0.110	0.106	0.106	0.112	0.093	0.090	0.082	0.090
Average values of viscosities (Pa · S)	0.108			0.109				0.089				

**Fig. 5.** Pore size distributions of matrices of the four castables.**Fig. 6.** Cumulative volume of specimens sintered at different temperatures as a function of pore diameter.

different (Table 1), and they have similar SIAC, resulting in similar viscosities of penetrated slag. Nevertheless, the median pore size of castable CLS70 is evidently smaller than that in the case of castable CLS90. This implies that the better slag penetration resistance of castable CLS70 than castable CLS90 is attributable to its smaller median pore size, which is related to the particle size distribution. Although the pore size distribution and

**Fig. 7.** Apparent porosities of castables and median pore sizes of matrices of castables.

median pore size of matrix of castable CFS70 are similar to those of castable CLS70, the higher SIAC of spinel LS70 (due to its greater lattice distortion) than spinel FS70 (Table 1), makes the penetrated slag more viscous in castable CLS70 than in castable CFS70. This explains why the slag penetration resistance of the latter is higher than that of the former.

The slag corrosion resistance depends on the dissolution rate of the castable in the slag, which is mainly determined by the spinel's grain size and the castable's chemical composition. Our previous work has found that smaller spinel grains had higher dissolution rates [21] and the dissolution rate of Al₂O₃-MgO refractories into the slag increases with an increase of the Al₂O₃ content in the refractories [22, 23]. The grain size (304 nm) of spinel LS70 is bigger than that of spinel LS78 or LS90, and the Al₂O₃ content in castable CLS70 is the lowest, therefore, castables CLS70 shows the highest corrosion resistance among the three castables (CLS70, CLS78 and CLS90). Although castables CLS70 and CFS70 have similar chemical compositions, spinel FS70 used in the latter has bigger grain size, therefore the latter shows slightly better corrosion resistance than the former.

Conclusions

Light-burned spinel can increase the slag penetration resistance of alumina-spinel castable more efficiently than fused spinel, if their chemical composition, particle size, lattice distortion and grain size are properly controlled.

The lattice distortion and particle size of spinel have strong effects on the slag penetration resistance of alumina-spinel castables. Spinel LS70, compared with spinel LS78 and LS90, has similar lattice distortion but the smallest particle size, resulting in the smallest pore size in the matrix of castable CLS70. On the other hand, compared with spinel FS70, it has greater lattice distortion and smaller particle size, result in the higher viscosities of penetrated slag and the smaller pore size in the matrix. So castable CLS70 shows the highest penetration resistance.

The chemical composition and grain size of spinel also show strong effects on the slag corrosion resistance of alumina-spinel castables. Spinel LS70 has greater grain size and lower Al₂O₃ content than spinel LS90, resulting in the slightly higher corrosion resistance of castable CLS70. On the other hand, compared with spinel FS70, spinel LS70 has similar chemical composition, but smaller grain size, thus resulting in the slightly lower corrosion resistance of castable CLS70.

Acknowledgments

The authors would like to thank the Shanghai Baosteel Industry Technological Service Co. Ltd., the 973 Program Earlier Research Project (No. 2012CB722702) and the School Foundation of Wuhan University of Science and Technology (No. 2012 × Z001) for financially supporting this work.

References

1. P. Korgul, D.R. Wilson, W.E. Lee, *J. Eur. Ceram. Soc.* 17 (1997) 77-84.
2. H. Sarpoolaky, S. Zhang, B.B. Argent, W.E. Lee, *J. Am. Ceram. Soc.* 84 (2001) 426-434.
3. L.A. Díaz, T. Torrecillas, A.H. Aza, P. Pena, *J. Eur. Ceram. Soc.* 27 (2007) 4623-4631.
4. S. Yilmaz, *Ironmak. Steelmak.* 33 (2006) 151-156.
5. S. Ghosh, T. Maiti, S. Sen, S. Mukhopadhyay, *Ceram. Int.* 31 (2005) 333-347.
6. S. Mukhopadhyay, P. Pal, B. Nag, P. Jana, *Ceram. Int.* 33 (2007) 175-186.
7. E.Y. Sako, M.A.L. Braulio, V.C. Pandolfelli, *Ceram. Int.* 38 (2012) 4783-4789.
8. A.P. Luz, M.A.L. Braulio, A.G. Tomba Martinez, V.C. Pandolfelli, *Ceram. Int.* 38 (2012) 1497-1505.
9. A.P. Luz, A.G. Tomb Martinez, M.A.L. Braulio, V.C. Pandolfelli, *Ceram. Int.* 37 (2011) 1191-1201.
10. Y. Ko, *J. Am. Ceram. Soc.* 83 (2000) 2333-2335.
11. Y. Ko, *Ceram. Int.* 28 (2002) 805-810.
12. S. Mukhopadhyay, T.K. Pal, P.K. DasPoddar, *Ceram. Int.* 35 (2009) 373-380.
13. S. Mukhopadhyay, P.K. DasPoddar, *Ceram. Int.* 30 (2004) 369-380.
14. W. Yan, N. Li, B. Han, *Int. J. Appl. Ceram. Technol.* 5 (2008) 633-640.
15. W. Yan, N. Li, B.Q. Han, *Sci. Sinter.* 41 (2009) 275-281.
16. W. Yan, N. Li, B. Han, *Interceram: Refractories Manual*, (2009) 25-28.
17. W. Yan, N. Li, B. Han, X. Fang, G. Liu, *Ceram-Silikáty* 54 (2010) 315-319.
18. W. Yan, N. Li, Z. Miao, G. Liu, Y. Li, *J. Ceram. Process. Res.* 13 (2012) 278-282.
19. N. Li, H. Gu, H. Zhao, in "Refractories Fundamental and Technology" Metallurgical Industry Press (2010) 9.
20. W. Yan, H. Luo, J. Tong, N. Li, *Int. J. Mater. Res.* 103 (2012) 1239-1243.
21. X. Fang, N. Li, W. Yan, *Naihuo Cailiao*, 45 (2011) 14-17.
22. M.K. Cho, G.G. Hong, S.K. Lee, *J. Eur. Ceram. Soc.* 22 (2002) 1783-1790.
23. H. Sarpoolaky, S. Zhang, W.E. Lee, *J. Eur. Ceram. Soc.* 23 (2003) 293-300.